# 3D structure-property correlations of electronic and energy materials by tomographic atomic force microscopy

Cite as: Appl. Phys. Lett. **118**, 080501 (2021); https://doi.org/10.1063/5.0040984 Submitted: 18 December 2020 • Accepted: 08 February 2021 • Published Online: 24 February 2021

🗓 Jingfeng Song, 厄 Yuanyuan Zhou and 🗓 Bryan D. Huey







### ARTICLES YOU MAY BE INTERESTED IN

Phase transformations and hysteresis in Si-based anode materials
Applied Physics Letters 118, 090501 (2021); https://doi.org/10.1063/5.0031416

How good are 2D transistors? An application-specific benchmarking study Applied Physics Letters 118, 030501 (2021); https://doi.org/10.1063/5.0029712

Spectral imaging of flexible terahertz coding metasurface
Applied Physics Letters 118, 081101 (2021); https://doi.org/10.1063/5.0043481

☐ QBLOX



Shorten Setup Time
Auto-Calibration
More Qubits

Fully-integrated
Quantum Control Stacks
Ultrastable DC to 18.5 GHz
Synchronized <<1 ns
Ultralow noise



100s qubits

visit our website >



# 3D structure-property correlations of electronic and energy materials by tomographic atomic force microscopy

Cite as: Appl. Phys. Lett. 118, 080501 (2021); doi: 10.1063/5.0040984 Submitted: 18 December 2020 · Accepted: 8 February 2021 · Published Online: 24 February 2021









Jingfeng Song,<sup>1,a)</sup> 🕞 Yuanyuan Zhou,<sup>2</sup> 🕞 and Bryan D. Huey<sup>1</sup> 🕞



## **AFFILIATIONS**

Department of Materials Science and Engineering, University of Connecticut, Storrs, Connecticut 06269, USA

### **ABSTRACT**

The ever-increasing complexity in the structure and design of functional materials systems and devices necessitates new imaging approaches with 3D characterization capabilities and nanoscale resolution. This Perspective provides a brief review of the tomographic atomic force microscopy technique and its recent applications in the 3D nanocharacterization of energy and electronic materials including hybrid perovskites, CdTe, and ferroelectric BiFeO<sub>3</sub>, and filamentary resistive memories as model systems. We also propose several challenges and opportunities for further developing and applying this emerging approach for investigating fundamental and applied phenomena in a broader scope of functional materials.

Published under license by AIP Publishing. https://doi.org/10.1063/5.0040984

First introduced by Binning, Quate, and Gerber in 1986, atomic force microscopy (AFM) was a ground-breaking invention in the history of nanoscience and nanotechnology. AFM can provide images of surface features truly down to the atomic-scale, with vertical resolution in the picometers and lateral resolution typically ranging from angstroms to tens of nanometers depending on the surface and imaging conditions.<sup>1-3</sup> Following the introduction of AFM, along with scanning tunneling microscopy, near-field scanning optical microscopy, as well as other variations on these prototypical approaches, the development of a broad scanning probe microscopy (SPM) community opened a new window into the nanoscale phenomena. 4-12 Today, SPM has become increasingly routine and commercially available in numerous fields of research, including the foundational work of imaging and manipulating single molecules or cells $^{13}$  and individual atoms, $^{4,14}$  characterizing nanowires and nanotubes, $^{15-17}$  studying twodimensional materials, 18,19 and monitoring materials in situ.5

As illustrated in the schematic of Fig. 1(a), the most common AFM implements rastering a fine tip across the sample surface, while maintaining a constant force ("DC" or "contact" mode), force gradient ("AC" or "Tapping" mode), or resonant frequency ("FM"). The tip is located near the end of a cantilever, and forces are nearly always detected by a laser beam reflected from the cantilever. 1-3,21 Until now, numerous previous reviews have given comprehensive discussions on the basic science and applications of various AFM and SPM techniques.<sup>5–12</sup> Unsurprisingly, however, most of the highest-resolution AFM studies implement noncontact or other gentle interactions between the probe and sample in order to minimize force and friction during scanning and, thereby, limit damage or contamination of the sample and AFM tip. 1,3,8 In this work, we instead focus our discussion on tomographic atomic force microscopy (T-AFM), which counterintuitively implements contact-mode AFM with relatively high loads, at least periodically, in order to purposefully mill the surface using the tip. Combined with property mapping, T-AFM can site-selectively reveal originally subsurface features and even enables nanoscale tomography of materials properties. Following a brief introduction to the specific surface-property imaging modes implemented herein, this Perspective article then primarily focuses on state-of-the-art applications of T-AFM for volumetric nanoscale analyses and revealing 3D structure-property relationships, as demonstrated with fundamentally and technologically important materials systems including hybrid perovskites, CdTe, BiFeO<sub>3</sub>, and electronic interconnects. At the end of this Perspective, we also summarize the opportunities and major challenges for extending the current application of T-AFM on highly crystalline and rigid materials to a broader scope, such as soft matter, nonconventional nanostructures (conductive domain walls and vortices), and 2D van der Waals layered materials.

<sup>&</sup>lt;sup>2</sup>Department of Physics, Hong Kong Baptist University, Kowloon, Hong Kong SAR, China

<sup>&</sup>lt;sup>a)</sup>Author to whom correspondence should be addressed: jingfeng.song@uconn.edu

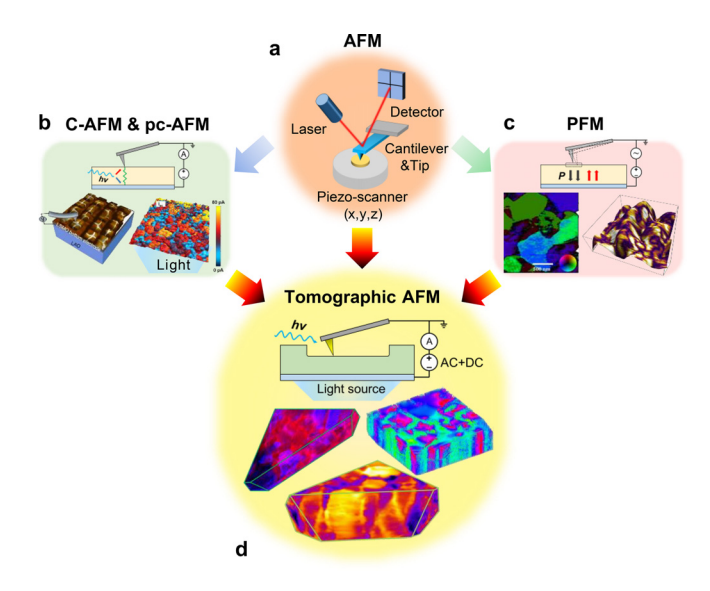


FIG. 1. (a)-(c) Schematic setups for AFM, C-AFM, pc-AFM, and PFM, with example images of surface characterizations of energy and electronic materials, including [panel (b) from left to right]: C-AFM image of ferroelectric domain wall conductivity of BiFeO<sub>3</sub>, reproduced with permission from Ma et al., Nat. Nanotechnol. 13, 947 (2018).<sup>25</sup> Copyright 2018 Springer Nature. pc-AFM mapping of photocurrent of the hybrid perovskite solar cell, reproduced with permission from Kutes et al., Nano Lett. 16, 3434 (2016).<sup>31</sup> Copyright 2016 American Chemical Society and [panel (c) from left to right] PFM image of ferroelectric domain orientation of a strontium bismuth tantalate (SBT) thin film, reproduced with permission from Gruverman et al., J. Mater. Sci. 41, 107 (2016). 36 Copyright 2016 Springer Nature and PFM image of ferroelectric domain contrast for a MAPbl<sub>3</sub> thin film, reprinted with permission from Kutes et al., J. Phys. Chem. Lett. 5, 3335 (2014).37 Copyright 2014 American Chemical Society. The lower panel in (d) shows the extension of these approaches into the third dimension, i.e., T-AFM, with example results such as the 3D and colocated short-circuit photocurrent and open circuit potential through operating a CdTe thin film solar cell (lower left), reprinted with permission from Atamanuk et al., Beilstein J. Nanotechnol. 9, 18029 (2018).38 Copyright 2018 Authors, licensed under a Creative Commons Attribution license. 3D ferroelectric domains of BiFeO<sub>3</sub> nanopillars within a magnetic CoFe<sub>2</sub>O<sub>4</sub> matrix in an epitaxial BiFeO<sub>3</sub>-CoFe<sub>2</sub>O<sub>4</sub> nanocomposite thin film (lower right) and 3D photocurrent distribution in a polycrystalline MAPbl<sub>3</sub> thin film (bottom).

The schematic of two representative contact-mode-based property mapping techniques that are frequently used for imaging energy and electronic materials is shown in Figs. 1(b) and 1(c). For instance, equipped with a conductive ultrasharp tip and an inline current detection circuit, conductive atomic force microscopy (C-AFM)<sup>22</sup> [Fig. 1(b)] is an essential tool for nanoscale mapping of local electrical properties. This includes DC current and *I-V* characteristics<sup>23–25</sup> with effective contact areas as small as 1 nm<sup>2.26,27</sup> The extension of C-AFM to photoconductive AFM (pc-AFM), via *in situ* sample illumination (usually obliquely or through a transparent substrate), also enables photoresponse studies relevant to solar cells, photodetectors, and LEDs. Examples include 2D semiconductors<sup>19</sup> and heterostructures<sup>28</sup> and traditional and new photovoltaics including silicon,<sup>29</sup> polymer/fullerene,<sup>30</sup> hybrid perovskites,<sup>31–33</sup> CdTe,<sup>34</sup> and GaN nanowire solar cells<sup>35</sup>

Distinct from conductive and photoconductive AFM, which mostly leverage the AFM probe as a moveable top electrode for DC or

AC measurements, piezoresponse force microscopy (PFM) instead typically interrogates the local nanomechanical response to electric fields via the converse piezoelectric effect, Fig. 1(c). In particular, when implementing AC fields and lock-in or related technologies, pm scale amplitudes and strong phase contrast (180° for oppositely oriented ferroelectric domains) are routinely achieved. 36,39,40 With the further development of dual AC resonance tracking PFM,  $^{41}$  high speed PFM,  $^{42,43}$  and band excitation PFM techniques,  $^{44}$  PFM has become an essential tool for locally identifying and manipulating the polarization status of both traditional and emerging piezoelectric and ferroelectric materials such as hybrid perovskites 37,45-48 and two-dimensional ferroelectrics. 49 By combining the local DC voltage polarizing via a conductive tip with serial high speed PFM imaging, ferroelectric domain switching movies with nanoscale spatial and down to 10 ns time resolution can be achieved, which enables direct observations of the origin and dynamics of domains switching of epitaxial Pb(Zr,Ti)O<sub>3</sub><sup>43,50</sup> and BiFeO<sub>3</sub>.<sup>51</sup> Additionally, AFM-probe-based ferroelectric-domain-patterning<sup>18</sup> has essentially provided a scientific playground for configuring the local polarization status of the ferroelectric gate dielectrics for multifunctional 2D optoelectronic <sup>19</sup> and nanoelectronic devices. <sup>1</sup>

By combining these nanoscale property-sensing AFM modes with AFM-tip-based milling, a trench is practically created during T-AFM, followed by repeated milling and planarizing of the specimen via serial or continuous in situ nanomachining. With this unconventional and progressive procedure, T-AFM can, therefore, provide data about previously buried features underneath the as-received sample surface and ultimately yield fully 3D tomograms<sup>53–56</sup> as demonstrated in Fig. 1(d) for energy and electronic materials. The spatial resolution of T-AFM is typically from 1 to 20 nm in the thickness direction, with similar dimensions laterally, over areas spanning 1–100  $\mu$ m<sup>2</sup>, throughout depths from several micrometers to a few nanometers. It is also generally compatible with commercial AFM systems, presuming either built-in or customized functional mapping capabilities, which often leverage tip or sample voltage control and/or other external stimuli (illumination, magnetic field, acoustics, etc.). The best examples thus far have focused on photoconductivities in solar cells (tomographic pc-AFM), 54,55,57 conduction pathways in electronic materials and interconnects (tomographic C-AFM), 53,56,58,59 and ferroelectric domain studies (tomographic PFM). 56,60 T-AFM is particularly promising for studying complex microstructures including superlattices, multiple phases, polycrystalline grains, and sub-granular effects such as domain walls or stacking faults.

Aside from C-AFM, pc-AFM, and PFM, there are numerous additional AFM variations for investigating functional materials such as magnetic force microscopy, <sup>61</sup> Kelvin probe force microscopy, <sup>62</sup> atomic force acoustic microscopy, <sup>63</sup> and scanning impedance microscopy, <sup>64</sup> which are effective for studying magnetic domains, <sup>65</sup> electrostatic surface potentials, <sup>66</sup> nanomechanical properties, <sup>63</sup> and local conductivity, respectively. <sup>67</sup> Each of these methods, and others, is compatible with tomographic AFM concepts as well. Regardless of the specific imaging method and contrast provided, there is a clear value of nanoscale volumetric property mapping with T-AFM, especially with the increasing miniaturization and microstructural complexity for functional devices. <sup>53–60</sup> In addition to the T-AFM approach, it is important to note that nano-x-ray computed tomography, and serial focused ion beam (FIB) sectioning along with SEM-based imaging, can provide complementary microstructural data with equivalent 3D

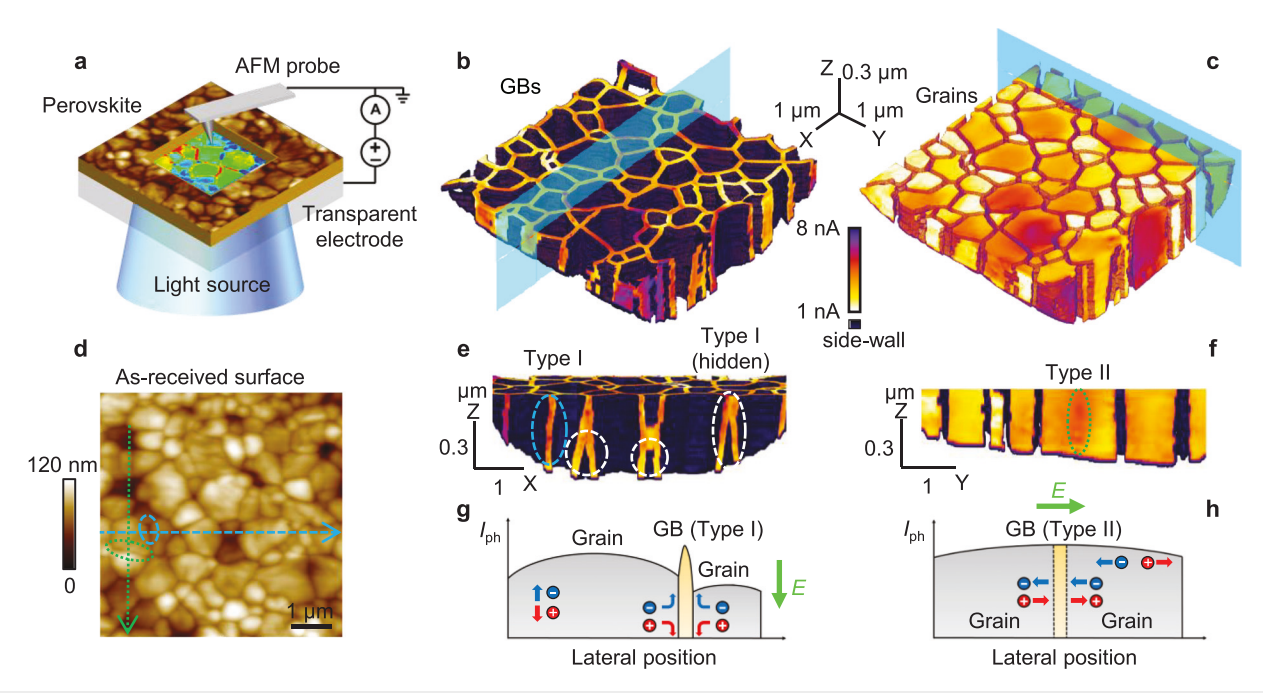


FIG. 2. (a) Schematic of tomographic pc-AFM measurement of a MAPbl<sub>3</sub> hybrid perovskite thin film. (b) and (c) 3D perspectives of the volumetric photocurrent digitally segmented into the conductive GB networks (b) and individual grains (c). (d) Topography of the as-received polycrystalline MAPbl<sub>3</sub>, with dashed and dotted oval overlays highlighting morphologically indistinguishable GBs that T-AFM reveals to be unique. (e) Cross-sectional tomogram (xz plane) where schematically indicated in (b) and also corresponding to the blue dashed line in (d). Overlays in (e) identify Type I GBs, some visible at the surface (blue ovals) and others diverging subsurface (white ovals). (f) Cross-sectional tomogram (yz plane) where indicated in (c), and along green dotted line in (d), where the dashed oval now highlights a typical Type II GB. (g) and (h) Charge transfer models depicting photogenerated charge transfer for highly conductive Type I (g) and conductively benign Type II (h) GBs. Reproduced with permission from Song et al., Nat. Commun. 11(1), 3308 (2020). COpyright 2020 Authors, licensed under a Creative Commons Attribution (CC BY) license.

resolution as T-AFM. There are already several examples of high precision nanofabrication<sup>68,69</sup> and 3D detection and composition profiling based on combining these techniques with conventional AFM. However, truly nanoscale x-ray-based tomography can be prohibitively expensive as it practically requires beam-line facilities, and FIB is known to possibly induce property-inhibiting side effects<sup>57</sup> due to ion implantation,<sup>71</sup> subsurface amorphization,<sup>68</sup> undesired surface topographies,<sup>70</sup> and other mechanisms.<sup>72</sup> Power or wavelength modulated thermal or optical excitation, respectively, can also provide some insight about subsurface features, 73-76 while transmission electron microscopy cross sections are now routinely employed for 2D snapshots,<sup>77,78</sup> but neither approach fully maps properties in all three dimensions. Furthermore, earlier tomography works under other terms, such as nanotomography<sup>79</sup> and SPM tomography,<sup>80</sup> have demonstrated volumetric imaging in thermoplastic polymers based on alternating between topography mapping and conventional material removal procedures such as repeating wet or plasma etching followed by SPM imaging<sup>79</sup> and ultramicrotome abrasion.<sup>81</sup> Although these methods are more cumbersome than simply using the conductive diamond tip as a scalpel to perform well-controlled material removal during continuous scans as in the T-AFM and AFM tomography or scalpel SPM<sup>53,82</sup> described herein, they may be more applicable especially to soft matter.

The most recent example of T-AFM is with hybrid perovskites, summarized in Fig. 2, which displays the first 3D photocurrent distribution throughout a methylammonium lead iodide (CH<sub>3</sub>NH<sub>3</sub>PbI<sub>3</sub> or

MAPbI<sub>3</sub>) thin film.<sup>54</sup> Ever since their first introduction as a promising light absorber for solar cells in 2009,83 hybrid perovskites have attracted enormous attention due to their unique organic-inorganic hybrid structures, superior optoelectronic properties, and low-cost manufacturability.<sup>84</sup> In just over one decade, hybrid perovskite solar cells have achieved a record certified power conversion efficiency of 25.2%, already surpassing that of polycrystalline silicon solar cells, which represent the culmination of five decades of extensive research and development and a commercial installation base contributing hundreds of terrawatts to the world's energy supply.<sup>85,86</sup> Tandem cells combining distinct layers of monocrystalline silicon and a hybrid perovskite thin film are even more promising, with a just announced 29.15% efficiency.<sup>87</sup> The MAPbI<sub>3</sub> films in these and other hybridperovskite-based optoelectronic architectures are nearly always polycrystalline, with grain sizes ranging from 100 nm to a few micrometers. They, therefore, comprise very high densities of grain boundaries (GBs) compared to most other high-performance photovoltaics,<sup>8</sup> obviating the need for fully characterizing the effects of such GBs on photogenerated carriers.<sup>86</sup> At present, most experimental approaches for studying photovoltaic performance at GBs are limited to surface sensitivities. This may be one of the critical reasons for the ongoing debate and contrasting evidence about whether GBs in hybrid perovskite solar cells are detrimental, benign, or beneficial.89

Figure 2(a) outlines the tomographic pc-AFM with a MAPbI<sub>3</sub> thin film grown on fluorine-doped tin oxide (FTO) glass, incorporating *in situ* illumination to facilitate photoconductivity studies as a

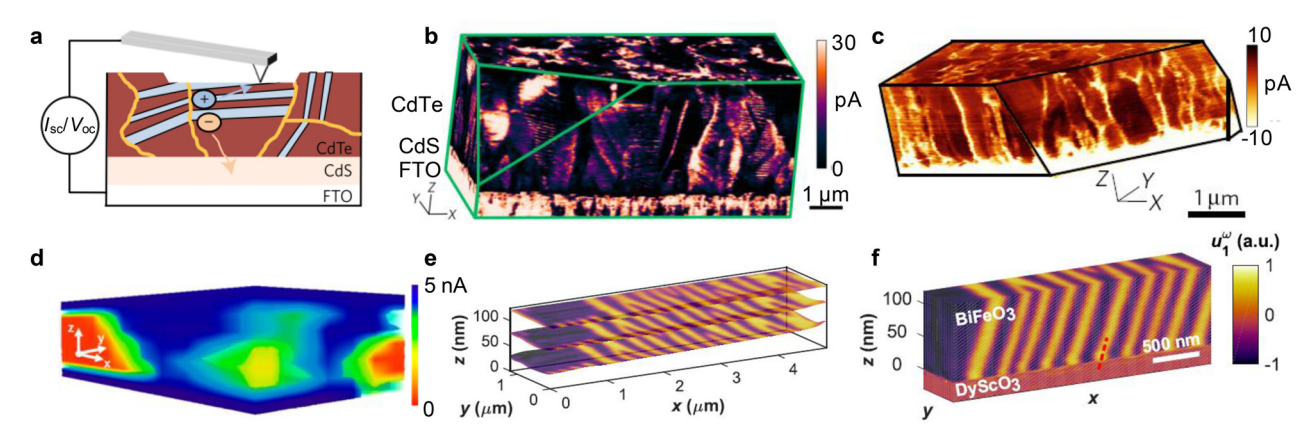


FIG. 3. (a) Schematic view of the tomographic pc-AFM measurement of short-circuit photocurrent or open voltage of CdTe solar cells. (b) Short-circuit photocurrent tomography of the CdTe polycrystalline thin film solar cell. (c) Charge transport in cadmium chloride treated CdTe at 0.7 V tip bias, near open-circuit condition. (d) First 3D reconstruction of a nanoscale conductive filament in a resistive memory device via tomographic C-AFM. (e) PFM piezoresponse superimposed onto surface topography of a 160 nm epitaxial BiFeO<sub>3</sub> thin film for three discrete steps during a T-AFM measurement. (f) Topographically reconstructed 3D thickness-resolved piezoresponse from a subregion of (e). (a)–(c) Reproduced with permission from Luria et al., Nat. Energy 1, 16150 (2016). Copyright 2016 Springer Nature. (d) Reproduced with permission from Celano et al., Nano Lett. 14, 2401 (2014). Copyright 2014 American Chemical Society. (e) and (f) Reproduced with permission from Steffes et al., Proc. Natl. Acad. Sci. U. S. A. 116, 2413 (2019). Copyright 2019 Authors, licensed under a Creative Commons Attribution-NonCommercial-NoDerivatives license 4.0 (CC BY-NC-ND).

function of microstructural features in 3D. The full tomogram, which is reconstructed from  $\sim$ 7.6  $\times$  10<sup>6</sup> data points and reveals originally subsurface contrast, is here digitally segmented into clearly enhanced 3D photocurrent networks along GBs [Fig. 2(b)] and grain-dependent photocurrents in Fig. 2(c). By thoroughly analyzing the photoconduction along the GBs, two distinct types of GBs, which are morphologically indistinguishable at the original film surface, were identified in Fig. 2(d). Type I GBs are predominant, exhibiting enhanced photoconductivities due to higher calculated effective mobilities [Fig. 2(e)]. Type II GBs are also occasionally present, though they are almost "invisible" compared to the photocurrent contrast in adjacent grains [Fig. 2(f)]. Mechanisms for charge transport along or across these type I and II GBs are depicted in Figs. 2(g) and 2(h) and suggest that future manufacturing control of the proportions of such interfaces could be beneficial for optimizing normal- and laterally configured devices, respectively. Such insight into conduction pathways for hybrid perovskites, which oftentimes are referred to as "soft" crystals 93,94 or even "polar-liquid-like," are particularly challenging due to the easily damaged microstructure and properties during conventional electron or ion beam-based investigations.<sup>20</sup> This first T-AFM study on the promising hybrid perovskite materials system thus provides a unique perspective for identifying and ultimately optimizing 3D structureproperty correlations in hybrid perovskite devices.

The applications of tomographic AFM to other inorganic systems are depicted in Fig. 3, including cadmium telluride (CdTe) solar cells, <sup>55</sup> resistive memory devices, <sup>53,58,59</sup> and BiFeO<sub>3</sub> epitaxial thin films and nanocomposites. <sup>56,60</sup> For instance, standard pc-AFM measurements on the top surface of a CdTe solar cell reveal spatially dependent short circuit currents and open circuit voltages akin to measurements on polycrystalline silicon cells. However, tomographic pc-AFM [Fig. 3(a)] of short-circuit photocurrents displays something different—that interconnected planar defects [inter- and intra-granular bands in Fig. 3(b)] are acting as preferred conduction pathways for holes.

Conversely, imaging near open circuit voltage conditions in Fig. 3(c) shows that grain boundaries provide spatially and energetically segregated conduction pathways for electrons.<sup>55</sup> This is contrary to the widely recognized detrimental role of grain boundaries as well as planar defects in polycrystalline thin-film solar cells, instead suggesting that interconnected planar defects and grain boundaries are highly beneficial for CdTe solar cells. 96 In one of the first demonstrations of a tomographic AFM approach, studying a resistive memory with C-AFM, Celano et al. identified nanoscale conductive filaments [Fig. 3(d)]. Along with similar reports on electronic interconnects, these 3D AFM approaches were proved to be valuable for investigating otherwise experimentally elusive phenomena, again due to the challenges of nanoscale volumetric property mapping.5 <sup>97</sup> Another high resolution study published thus far implemented tomographic PFM to map ferroelectric domains repeatedly throughout the depth of an epitaxial BiFeO<sub>3</sub> thin film [Fig. 3(e)]. Voxels finer than 315 nm<sup>3</sup> were achieved, with a depth resolution of just 0.97 nm confirmed by the abrupt loss of PFM contrast upon reaching the nonferroelectric underlying electrode and substrate [Fig. 3(f)]. Again, the 3D tomograms clearly uncover what is hidden beneath the surface—a 40° tilt of the ferroelectric domain walls from the [100] pseudocubic crystal axis of BiFeO<sub>3</sub>. Some domain walls also converge or diverge beneath the surface, akin to similar observations for grain boundaries in solar cells such as with MAPbI<sub>3</sub> in Figs. 2(e) and 2(f).

In addition to volumetric insights, the T-AFM approach can provide several further benefits, specifically for delicate and controllable nanomilling or nanopolishing, as is demonstrated in Fig. 4. Programmable shapes such as a thickness gradient can be prepared for further study via AFM tip-based milling of, e.g., a wedge configuration [Fig. 4(a)]. Clearly, this process is not strictly damage free, and certainly not non- or minimally invasive as is usually the unwritten rule of SPM based studies. For some materials systems, though, any damage is isolated to the excavated material, which is then continually

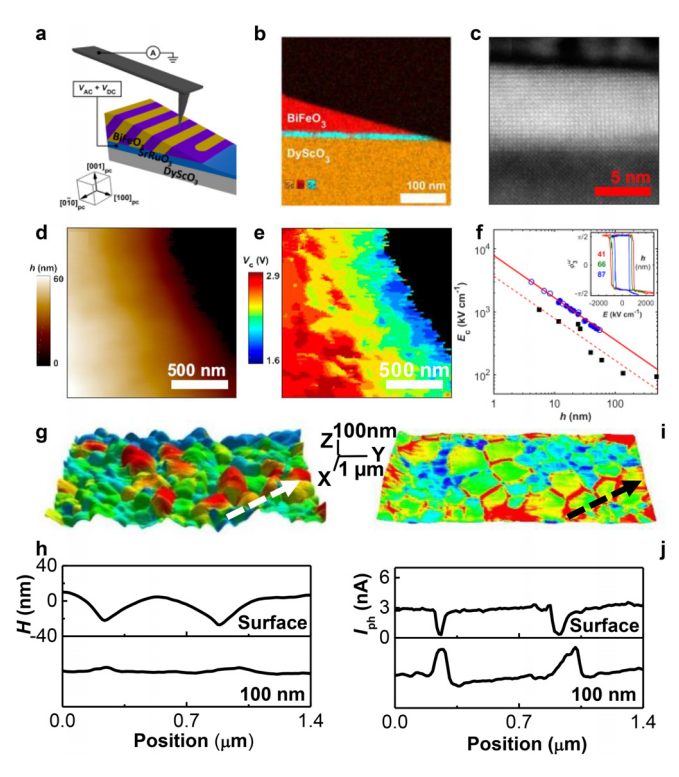


**FIG. 4.** (a) Schematic of T-AFM nanomilling of BiFeO $_3$  forming a nanowedge region with BiFeO $_3$  and SrRuO $_3$  and stripe-type contrast in BiFeO $_3$  represents ferroelectric domains. (b) and (c) Cross-sectional TEM image of BiFeO $_3$  following T-AFM nanomilling showing unperturbed crystal structure. (d) AFM topography of the nanowedge region produced by T-AFM nanomilling. (e) and (f) Map of the coercive voltage  $V_c$  at varying thickness on a wedge region of the BiFeO $_3$  film, with numerical fitting of the coercive field with respect to the BiFeO $_3$  thin film thickness. (g)–(j) pc-AFM images superimposed with surface topography of MAPbl $_3$  thin film before (g) and (h) and after (i) and (j) T-AFM nanomachining. (a)–(f) Reproduced with permission from Steffes et al., Proc. Natl. Acad. Sci. U. S. A. **116**, 2413 (2019). Copyright 2019 Authors, licensed under a Creative Commons Attribution-NonCommercial-NoDerivatives license 4.0 (CC BY-NC-ND). (g)–(i) Reproduced with permission from Song et al., Nat. Commun. **11**(1), 3308 (2020). Copyright 2020 Authors, licensed under a Creative Commons Attribution (CC BY) license.

swept away by the rastering probe, while the underlying crystal structure and properties remain unperturbed. For example, in follow-up cross-sectional TEM studies in Figs. 4(b) and 4(c), BiFeO<sub>3</sub> beneath the polished surface does not exhibit dislocations and as shown here for BiFeO<sub>3</sub> atomic columns remain even down to a milled film thickness of less than 7 nm [Fig. 4(c)]. 56 This conveniently facilitates investigations of size or thickness-dependent properties, emergent properties, and/or isolation of otherwise interconnected features—all in a single field of view instead of from multiple specimens that ideally but in reality are seldom free of inadvertent fluctuations in structure and composition.<sup>56,57</sup> For instance, a thickness gradient in BiFeO<sub>3</sub> [Fig. 4(d)] enables high resolution mapping of the coercive bias over the range of 1-60 nm of ferroelectric thin film, which uniquely provides high fidelity statistics on the coercive field for polarization vs thickness [Figs. 4(e) and 4(f)]. This study conclusively and somewhat surprisingly proves that domain switching obeys Kay-Dunn scaling. Finally, simple planarization can itself be highly beneficial, for instance, to diminish surface roughness in order to eliminate topography or surface-facet induced artifacts.  $^{54,57,60}$  For instance, for the hybrid perovskite thin film, T-AFM based nanopolishing diminished the asgrown surface roughness over an order of magnitude to less than 2 nm root mean square roughness [Figs. 4(g) and 4(h)]. This reveals a clear inversion in photoconduction at GBs, from apparently diminished for the as-provided rough surface to absolutely enhanced for the smoothed material [Figs. 4(i) and 4(j)]. With removal down to unit-cell-thick layers already demonstrated,  $^{56}$  T-AFM and the AFM-tip based nanomilling that it leverages are, therefore, promising for a wide range of investigations into devices that exhibit three-dimensional architectures and/or sensitivities.

Tomographic AFM and the related nanomachining approach so far have been focused on investigating highly crystalline and relatively rigid materials (e.g., perovskite thin films, functional nanocomposites, complex oxides, and superlattices). There are still numerous exciting areas for future explorations with T-AFM. For instance, volumetric property mapping of soft matter, photogenerated carrier transfer inside fully assembled perovskite and organic solar cells, volumetric mapping of mechanical properties of biomaterials, thinning and nanopatterning of 2D layered semiconductors and multiferroics, and 3D high-resolution imaging of emergent nonconventional nanostructures such as conductive ferroelectric domain walls<sup>25</sup> and vortices.

For these possible further applications of T-AFM, there are still significant challenges need to be resolved. For soft materials, such as amorphous or partially crystallized polymer, conducting high fidelity AFM imaging with controllable materials removal and no significant altering of the remaining sample is still an open question calling for more future work. Until now, some encouraging results have been reported on polyvinylidene fluoride (PVDF)-based ferroelectric polymer. For example, mechanical-force-induced ferroelectric polarization switching<sup>99</sup> and surface mechanical-annealing-controlled local piezoresponse enhancement<sup>100</sup> have been demonstrated via high-load AFM local probing and PFM scans on soft PVDF films. These results make it promising for the T-AFM approach to "dig deeper" with soft materials, especially with electroactive or photoactive polymers to explore the depth-dependent properties (piezoresponse, ferroelectricity, domain walls, and photoresponse). So far, volumetric mapping of these properties with electron-beam based techniques is still challenging due to the possible fast decay of polymer under focused high energy beams. Although 2D high-resolution nanomechanical property mapping of metal and soft biomaterials has been demonstrated with atomic force acoustic microscopy,63 developing a feasible material removal procedure during imaging in acoustic mode and in situ conversion of the AFM signal to actual mechanical constants are critical to achieve 3D volumetric imaging of mechanical properties. For emergent nonconventional nanostructures such as conductive ferroelectric domain walls and vortices, the actual lateral feature scales [e.g., down to around 3 nm for the ferroelectric domain wall of Pb(Zr,Ti)O<sub>3</sub><sup>101</sup> and around 6 nm for vortices in SrTiO<sub>3</sub>/PbTiO<sub>3</sub> superlattices<sup>102</sup>] are imposing great challenge for T-AFM, as these values are approaching the limit of the SPM imaging resolution and the current T-AFM voxel size.<sup>5</sup> In this sense, an optimized T-AFM approach with much higher spatial resolution could be the first step toward resolving this challenge. Furthermore, angstrom-level, "smart" nanomachining with optimal fully 3D precision by an active feedback procedure can be used to achieve room temperature nanopatterning of electroactive or

photoactive polymers, which could be an unique alternative to the conventional optical/electron-beam lithography or nanoimprint lithography approach at elevated temperatures. <sup>104</sup> Additionally, for 2D van der Waals layered materials, although only AFM-tip-controlled twisting and sliding of 2D boron nitride <sup>105</sup> and AFM-assisted thermal nanolithography of low-dimensional nanoelectronics <sup>106,107</sup> have been demonstrated so far, programmable T-AFM nanomachining may be useful to ultimately achieve lithography-free and thinning and machining of 2D layers locally with a rastering AFM tip, rather than using traditional mechanical exfoliation or high energy pulse laser thinning methods. <sup>108</sup>

In summary, tomographic AFM approaches have proven to be unique and promising tools for 3D correlations between structure and materials properties. With *in situ* and *in operando* compatibility and the entire family of AFM-based measurement modalities available, there are numerous potential applications of this powerful technique. In particular, when complemented by electron and ion beam studies, diffraction measurements, and/or optical interrogation, T-AFM is certain to yield new perspectives into fundamental properties of 3D structured materials and their optimized applications.

J.S. and B.D.H. recognize support from the Institute of Materials Science, University of Connecticut, and from the NSF (MRI development award, No. DMR-1726862). Y.Z. acknowledges the support of startup grants from the Department of Physics, Faculty of Science, and Research Committee of the Hong Kong Baptist University.

### DATA AVAILABILITY

The data that support the findings of this study are available from the corresponding author upon reasonable request.

# REFERENCES

- <sup>1</sup>G. Binnig, C. F. Quate, and C. Gerber, Phys. Rev. Lett. **56**(9), 930 (1986).
- <sup>2</sup>G. Binnig, C. Gerber, E. Stoll, T. R. Albrecht, and C. F. Quate, Europhys. Lett. 3(12), 1281 (1987).
- <sup>3</sup>B. D. Huey, J. Luria, and D. A. Bonnell, in *Springer Handbook of Microscopy*, edited by P. W. Hawkes and J. C. H. Spence (Springer International Publishing, Cham, 2019), p. 1239.
- <sup>4</sup>C. Gerber and H. P. Lang, Nat. Nanotechnol. 1(1), 3 (2006).
- <sup>5</sup>R. Berger, A. L. Domanski, and S. A. L. Weber, Eur. Polym. J. **49**(8), 1907 (2013).
- <sup>6</sup>F. J. Giessibl, Rev. Mod. Phys. 75(3), 949 (2003).
- <sup>7</sup>F. Hui and M. Lanza, Nat. Electron. 2(6), 221 (2019).
- <sup>8</sup>Y. F. Dufrêne, T. Ando, R. Garcia, D. Alsteens, D. Martinez-Martin, A. Engel, C. Gerber, and D. J. Müller, Nat. Nanotechnol. 12(4), 295 (2017).
- <sup>9</sup>N. Jalili and K. Laxminarayana, Mechatronics 14(8), 907 (2004).
- 10 D. J. Müller and Y. F. Dufrêne, Trends Cell Biol. 21(8), 461 (2011).
- <sup>11</sup>A. N. Patel and C. Kranz, Annu. Rev. Anal. Chem. 11(1), 329 (2018).
- <sup>12</sup>S. Liu and Y. Wang, in *Advances in Food and Nutrition Research*, edited by S. L. Taylor (Academic Press, 2011), Vol. 62, p. 201.
- <sup>13</sup>M. Radmacher, R. W. Tillamnn, M. Fritz, and H. E. Gaub, Science 257(5078), 1900 (1992).
- <sup>14</sup>N. Oyabu, Ó. Custance, I. Yi, Y. Sugawara, and S. Morita, Phys. Rev. Lett. 90(17), 176102 (2003).
- <sup>15</sup>M.-H. Zhao, Z.-L. Wang, and S. X. Mao, Nano Lett. 4(4), 587 (2004).
- <sup>16</sup>Z. L. Wang and J. Song, Science **312**(5771), 242 (2006).
- <sup>17</sup>J. F. Campbell, I. Tessmer, H. H. Thorp, and D. A. Erie, J. Am. Chem. Soc. 130(32), 10648 (2008).
- <sup>18</sup>Z. Y. Xiao, J. F. Song, D. K. Ferry, S. Ducharme, and X. Hong, Phys. Rev. Lett. 118(23), 236801 (2017).

- <sup>19</sup>L. Lv, F. Zhuge, F. Xie, X. Xiong, Q. Zhang, N. Zhang, Y. Huang, and T. Zhai, Nat. Commun. 10(1), 3331 (2019).
- <sup>20</sup>E. M. Tennyson, T. A. S. Doherty, and S. D. Stranks, Nat. Rev. Mater. 4(9), 573 (2019).
- <sup>21</sup>R. B. Marcus, T. S. Ravi, T. Gmitter, K. Chin, D. Liu, W. J. Orvis, D. R. Ciarlo, C. E. Hunt, and J. Trujillo, Appl. Phys. Lett. **56**(3), 236 (1990).
- <sup>22</sup>M. P. Murrell, M. E. Welland, S. J. O'Shea, T. M. H. Wong, J. R. Barnes, A. W. McKinnon, M. Heyns, and S. Verhaverbeke, Appl. Phys. Lett. 62(7), 786 (1993)
- <sup>23</sup>A. Gruverman, D. Wu, H. Lu, Y. Wang, H. W. Jang, C. M. Folkman, M. Y. Zhuravlev, D. Felker, M. Rzchowski, C. B. Eom, and E. Y. Tsymbal, Nano Lett. 9(10), 3539 (2009).
- <sup>24</sup>J. Seidel, L. W. Martin, Q. He, Q. Zhan, Y. H. Chu, A. Rother, M. E. Hawkridge, P. Maksymovych, P. Yu, M. Gajek, N. Balke, S. V. Kalinin, S. Gemming, F. Wang, G. Catalan, J. F. Scott, N. A. Spaldin, J. Orenstein, and R. Ramesh, Nat. Mater. 8(3), 229 (2009).
- <sup>25</sup>J. Ma, J. Ma, Q. Zhang, R. Peng, J. Wang, C. Liu, M. Wang, N. Li, M. Chen, X. Cheng, P. Gao, L. Gu, L.-Q. Chen, P. Yu, J. Zhang, and C.-W. Nan, Nat. Nanotechnol. 13(10), 947 (2018).
- <sup>26</sup>U. Celano, T. Hantschel, G. Giammaria, R. C. Chintala, T. Conard, H. Bender, and W. Vandervorst, J. Appl. Phys. 117(21), 214305 (2015).
- <sup>27</sup>C. Rodenbücher, G. Bihlmayer, W. Speier, J. Kubacki, M. Wojtyniak, M. Rogala, D. Wrana, F. Krok, and K. Szot, Nanoscale 10(24), 11498 (2018).
- <sup>28</sup>F. Giannazzo, G. Greco, F. Roccaforte, C. Mahata, and M. Lanza, in *Electrical Atomic Force Microscopy for Nanoelectronics*, edited by U. Celano (Springer International Publishing, Cham, 2019), p. 303.
- <sup>29</sup>P. Narchi, J. Alvarez, P. Chrétien, G. Picardi, R. Cariou, M. Foldyna, P. Prod'homme, J.-P. Kleider, and P. R. i Cabarrocas, Nanoscale Res. Lett. 11(1), 55 (2016).
- <sup>30</sup>D. C. Coffey, O. G. Reid, D. B. Rodovsky, G. P. Bartholomew, and D. S. Ginger, Nano Lett. 7(3), 738 (2007).
- <sup>31</sup>Y. Kutes, Y. Zhou, J. L. Bosse, J. Steffes, N. P. Padture, and B. D. Huey, Nano Lett. 16(6), 3434 (2016).
- <sup>32</sup>C. Stavrakas, A. A. Zhumekenov, R. Brenes, M. Abdi-Jalebi, V. Bulović, O. M. Bakr, E. S. Barnard, and S. D. Stranks, Energy Environ. Sci. 11(10), 2846 (2018)
- 33B. Huang, G. Kong, E. N. Esfahani, S. Chen, Q. Li, J. Yu, N. Xu, Y. Zhang, S. Xie, H. Wen, P. Gao, J. Zhao, and J. Li, npj Quantum Mater. 3(1), 30
- <sup>34</sup>M. S. Leite, M. Abashin, H. J. Lezec, A. Gianfrancesco, A. A. Talin, and N. B. Zhiteney, ACS Nano 8(11), 11883 (2014).
- <sup>35</sup>S. L. Howell, S. Padalkar, K. Yoon, Q. Li, D. D. Koleske, J. J. Wierer, G. T. Wang, and L. J. Lauhon, Nano Lett. 13(11), 5123 (2013).
- <sup>36</sup>A. Gruverman and S. V. Kalinin, J. Mater. Sci. **41**(1), 107 (2006).
- <sup>37</sup>Y. Kutes, L. Ye, Y. Zhou, S. Pang, B. D. Huey, and N. P. Padture, J. Phys. Chem. Lett. 5(19), 3335 (2014).
- <sup>38</sup>K. Atamanuk, J. Luria, and B. D. Huey, Beilstein J. Nanotechnol. 9, 1802 (2018).
- <sup>39</sup>O. Kolosov, A. Gruverman, J. Hatano, K. Takahashi, and H. Tokumoto, Phys. Rev. Lett. 74(21), 4309 (1995).
- <sup>40</sup>S. V. Kalinin and D. A. Bonnell, Phys. Rev. B **65**(12), 125408 (2002).
- <sup>41</sup>B. J. Rodriguez, C. Callahan, S. V. Kalinin, and R. Proksch, Nanotechnology 18(47), 475504 (2007).
- <sup>42</sup>R. Nath, Y.-H. Chu, N. A. Polomoff, R. Ramesh, and B. D. Huey, Appl. Phys. Lett. 93(7), 072905 (2008).
- <sup>43</sup>B. D. Huey, R. Nath Premnath, S. Lee, and N. A. Polomoff, J. Am. Ceram. Soc. 95(4), 1147 (2012).
- <sup>44</sup>S. Jesse, S. V. Kalinin, R. Proksch, A. P. Baddorf, and B. J. Rodriguez, Nanotechnology 18(43), 435503 (2007).
- <sup>45</sup>J. Song, Z. Xiao, B. Chen, S. Prockish, X. Chen, A. Rajapitamahuni, L. Zhang, J. Huang, and X. Hong, ACS Appl. Mater. Interfaces 10(22), 19218 (2018).
- 46 H. Röhm, T. Leonhard, M. J. Hoffmann, and A. Colsmann, Energy Environ. Sci. 10(4), 950 (2017).
- <sup>47</sup>H.-Y. Zhang, X.-J. Song, X.-G. Chen, Z.-X. Zhang, Y.-M. You, Y.-Y. Tang, and R.-G. Xiong, J. Am. Chem. Soc. 142, 4925 (2020).
- 48H.-Y. Ye, Y.-Y. Tang, P.-F. Li, W.-Q. Liao, J.-X. Gao, X.-N. Hua, H. Cai, P.-P. Shi, Y.-M. You, and R.-G. Xiong, Science 361(6398), 151 (2018).

- <sup>49</sup>F. Liu, L. You, K. L. Seyler, X. Li, P. Yu, J. Lin, X. Wang, J. Zhou, H. Wang, H. He, S. T. Pantelides, W. Zhou, P. Sharma, X. Xu, P. M. Ajayan, J. Wang, and Z. Liu, Nat. Commun. 7(1), 12357 (2016).
- <sup>50</sup>N. A. Polomoff, R. N. Premnath, J. L. Bosse, and B. D. Huey, J. Mater. Sci. 44(19), 5189 (2009).
- <sup>51</sup>J. T. Heron, J. L. Bosse, Q. He, Y. Gao, M. Trassin, L. Ye, J. D. Clarkson, C. Wang, J. Liu, S. Salahuddin, D. C. Ralph, D. G. Schlom, J. Íñiguez, B. D. Huey, and R. Ramesh, Nature 516(7531), 370 (2014).
- <sup>52</sup>G. Wu, B. Tian, L. Liu, W. Lv, S. Wu, X. Wang, Y. Chen, J. Li, Z. Wang, S. Wu, H. Shen, T. Lin, P. Zhou, Q. Liu, C. Duan, S. Zhang, X. Meng, S. Wu, W. Hu, X. Wang, J. Chu, and J. Wang, Nat. Electron. 3(1), 43 (2020).
- <sup>53</sup>U. Celano, L. Goux, A. Belmonte, K. Opsomer, A. Franquet, A. Schulze, C. Detavernier, O. Richard, H. Bender, M. Jurczak, and W. Vandervorst, Nano Lett. 14(5), 2401 (2014).
- 54 J. Song, Y. Zhou, N. P. Padture, and B. D. Huey, Nat. Commun. 11(1), 3308 (2020).
- 55]. Luria, Y. Kutes, A. Moore, L. Zhang, E. A. Stach, and B. D. Huey, Nat. Energy 1, 16150 (2016).
- <sup>56</sup>J. J. Steffes, R. A. Ristau, R. Ramesh, and B. D. Huey, Proc. Natl. Acad. Sci. 116(7), 2413 (2019).
- 57Y. Kutes, J. Luria, Y. Sun, A. Moore, B. A. Aguirre, J. L. Cruz-Campa, M. Aindow, D. Zubia, and B. D. Huey, Nanotechnology 28(18), 185705 (2017).
- <sup>58</sup>M. Buckwell, L. Montesi, S. Hudziak, A. Mehonic, and A. J. Kenyon, Nanoscale 7(43), 18030 (2015).
- <sup>59</sup>U. Celano, L. Goux, K. Opsomer, M. Iapichino, A. Belmonte, A. Franquet, I. Hoflijk, C. Detavernier, M. Jurczak, and W. Vandervorst, Microelectron. Eng. 120, 67 (2014).
- <sup>60</sup>J. Song, S. Zhuang, M. Martin, L. Ortiz, B. Paudel, D. Yarotski, J. Hu, A. Chen, and B. D. Huey, "Interfacial-strain-controlled ferroelectricity in self-assembled BiFeO<sub>3</sub> nanostructures," unpublished.
- 61 U. Hartmann, Annu. Rev. Mater. Sci. 29(1), 53 (1999).
- 62W. Melitz, J. Shen, A. C. Kummel, and S. Lee, Surf. Sci. Rep. 66(1), 1 (2011).
- 63 B. D. Huey, Annu. Rev. Mater. Res. 37(1), 351 (2007).
- 64S. V. Kalinin and D. A. Bonnell, MRS Proc. 699, R1.2 (2001).
- <sup>65</sup>A. Hirohata, M. Samiepour, and M. Corbetta, in *Electrical Atomic Force Microscopy for Nanoelectronics*, edited by U. Celano (Springer International Publishing, Cham, 2019), p. 231.
- 66 B. D. Huey, D. Lisjak, and D. A. Bonnell, J. Am. Ceram. Soc. 82(7), 1941 (1999).
- <sup>67</sup>X. Wu, U. Petralanda, L. Zheng, Y. Ren, R. Hu, S.-W. Cheong, S. Artyukhin, and K. Lai, Sci. Adv. 3(5), e1602371 (2017).
- <sup>68</sup>B. D. Huey and R. M. Langford, Nanotechnology **14**(3), 409 (2003).
- <sup>69</sup>K. Thompson, D. Lawrence, D. J. Larson, J. D. Olson, T. F. Kelly, and B. Gorman, Ultramicroscopy 107(2), 131 (2007).
- 70 L. Pillatsch, S. Kalácska, X. Maeder, and J. Michler, Microsc. Microanal. 2019, 1–9 (2020).
- <sup>71</sup>B. I. Prenitzer, C. A. Urbanik-Shannon, L. A. Giannuzzi, S. R. Brown, R. B. Irwin, T. L. Shofner, and F. A. Stevie, Microsc. Microanal. 9(3), 216 (2003).
- <sup>72</sup>J. Mayer, L. A. Giannuzzi, T. Kamino, and J. Michael, MRS Bull. 32(5), 400 (2007).
- <sup>73</sup>J. Song, H. Lu, A. Gruverman, and S. Ducharme, Appl. Phys. Lett. **104**(19), 192901 (2014).
- <sup>74</sup>C. Pham, A. Petre, L. Berquez, R. Flores-Suarez, A. Mellinger, W. Wirges, and R. Gerhard, IEEE Trans. Dielectr. Electr. Insul. 16(3), 676 (2009).
- <sup>75</sup>A. Haußmann, L. Kirsten, S. Schmidt, P. Cimalla, L. Wehmeier, E. Koch, and L. M. Eng, Ann. Phys. **529**(8), 1700139 (2017).
- <sup>76</sup>S. Cherifi-Hertel, H. Bulou, R. Hertel, G. Taupier, K. D. Dorkenoo, C. Andreas, J. Guyonnet, I. Gaponenko, K. Gallo, and P. Paruch, Nat. Commun. 8(1), 15768 (2017).
- <sup>77</sup>B. Yang, O. Dyck, J. Poplawsky, J. Keum, A. Puretzky, S. Das, I. Ivanov, C. Rouleau, G. Duscher, D. Geohegan, and K. Xiao, J. Am. Chem. Soc. 137(29), 9210 (2015).
- <sup>78</sup>C. Li, Y. Wu, J. Poplawsky, T. J. Pennycook, N. Paudel, W. Yin, S. J. Haigh, M. P. Oxley, A. R. Lupini, M. Al-Jassim, S. J. Pennycook, and Y. Yan, Phys. Rev. Lett. 112(15), 156103 (2014).
- <sup>79</sup>R. Magerle, Phys. Rev. Lett. **85**(13), 2749 (2000).

- <sup>80</sup> A. Alekseev, A. Efimov, J. Loos, N. Matsko, and J. Syurik, Eur. Polym. J. 52, 154 (2014).
- 81 A. E. Efimov, A. G. Tonevitsky, M. Dittrich, and N. B. Matsko, J. Microsc. 226(3), 207 (2007).
- <sup>82</sup>A. Schulze, T. Hantschel, A. Dathe, P. Eyben, X. Ke, and W. Vandervorst, Nanotechnology 23(30), 305707 (2012).
- <sup>83</sup>A. Kojima, K. Teshima, Y. Shirai, and T. Miyasaka, J. Am. Chem. Soc. 131(17), 6050 (2009).
- <sup>84</sup>M. A. Green, A. Ho-Baillie, and H. J. Snaith, Nat. Photonics **8**, 506 (2014).
- 85NREL, Best Research-Cell Efficiency Chart (2020).
- 86N.-G. Park, M. Grätzel, T. Miyasaka, K. Zhu, and K. Emery, Nat. Energy 1(11), 16152 (2016).
- 87 A. Al-Ashouri, E. Köhnen, B. Li, A. Magomedov, H. Hempel, P. Caprioglio, J. A. Márquez, A. B. Morales Vilches, E. Kasparavicius, J. A. Smith, N. Phung, D. Menzel, M. Grischek, L. Kegelmann, D. Skroblin, C. Gollwitzer, T. Malinauskas, M. Jošt, G. Matič, B. Rech, R. Schlatmann, M. Topič, L. Korte, A. Abate, B. Stannowski, D. Neher, M. Stolterfoht, T. Unold, V. Getautis, and S. Albrecht, Science 370(6522), 1300 (2020).
- <sup>88</sup>Y. Zhou, O. S. Game, S. Pang, and N. P. Padture, J. Phys. Chem. Lett. 6(23), 4827 (2015).
- 89 W.-J. Yin, T. Shi, and Y. Yan, Adv. Mater. 26(27), 4653 (2014).
- <sup>90</sup>J. S. Yun, A. Ho-Baillie, S. Huang, S. H. Woo, Y. Heo, J. Seidel, F. Huang, Y.-B. Cheng, and M. A. Green, J. Phys. Chem. Lett. 6(5), 875 (2015).
- <sup>91</sup>D. W. de Quilettes, S. M. Vorpahl, S. D. Stranks, H. Nagaoka, G. E. Eperon, M. E. Ziffer, H. J. Snaith, and D. S. Ginger, Science 348(6235), 683 (2015).
- <sup>92</sup>J.-W. Lee, S.-H. Bae, N. De Marco, Y.-T. Hsieh, Z. Dai, and Y. Yang, Mater. Today Energy 7, 149 (2018).
- <sup>93</sup>Q. F. Dong, J. F. Song, Y. J. Fang, Y. C. Shao, S. Ducharme, and J. S. Huang, Adv. Mater. 28(14), 2816 (2016).
- <sup>94</sup>B. Chen, T. Li, Q. Dong, E. Mosconi, J. Song, Z. Chen, Y. Deng, Y. Liu, S. Ducharme, A. Gruverman, F. D. Angelis, and J. Huang, Nat. Mater. 17(11), 1020 (2018).
- 95H. Zhu, K. Miyata, Y. Fu, J. Wang, P. P. Joshi, D. Niesner, K. W. Williams, S. Jin, and X. Y. Zhu, Science 353(6306), 1409 (2016).
- <sup>96</sup>I. Visoly-Fisher, S. R. Cohen, K. Gartsman, A. Ruzin, and D. Cahen, Adv. Funct. Mater. 16(5), 649 (2006).
- <sup>97</sup>P. Eyben, R. Ritzenthaler, A. D. Keersgieter, U. Celano, T. Chiarella, A. Veloso, H. Mertens, V. Pena, G. Santoro, J. Machillot, M. Kim, T. Miyashita, N. Yoshida, H. Bender, O. Richard, K. Paredis, L. Wouters, J. Mitard, and N. Horiguchi, paper presented at the 2019 IEEE International Electron Devices Meeting (IEDM), 2019.
- 98 R. Ramesh and D. G. Schlom, Nat. Rev. Mater. 4(4), 257 (2019).
- <sup>99</sup>X. Chen, X. Tang, X.-Z. Chen, Y.-L. Chen, X. Guo, H.-X. Ge, and Q.-D. Shen, Appl. Phys. Lett. **106**(4), 042903 (2015).
- 100 Y.-Y. Choi, P. Sharma, C. Phatak, D. J. Gosztola, Y. Liu, J. Lee, B. Lee, J. Li, A. Gruverman, S. Ducharme, and S. Hong, ACS Nano 9(2), 1809 (2015).
- <sup>101</sup>C.-L. Jia, K. W. Urban, M. Alexe, D. Hesse, and I. Vrejoiu, Science 331(6023), 1420 (2011).
- <sup>102</sup>A. K. Yadav, K. X. Nguyen, Z. Hong, P. García-Fernández, P. Aguado-Puente, C. T. Nelson, S. Das, B. Prasad, D. Kwon, S. Cheema, A. I. Khan, C. Hu, J. Iñiguez, J. Junquera, L.-Q. Chen, D. A. Muller, R. Ramesh, and S. Salahuddin, Nature 565(7740), 468 (2019).
- 103 W. Linthicum, W. P. Huey, and B. D. Huey, "Smart AFM nanolithography via nanoscale regressively adjusted setpoints (nRASP)," unpublished.
- 104J. Song, H. Lu, K. Foreman, S. Li, L. Tan, S. Adenwalla, A. Gruverman, and S. Ducharme, J. Mater. Chem. C 4(25), 5914 (2016).
- 105R. Ribeiro-Palau, C. Zhang, K. Watanabe, T. Taniguchi, J. Hone, and C. R. Dean, Science 361(6403), 690 (2018).
- <sup>106</sup>X. Liu, S. T. Howell, A. Conde-Rubio, G. Boero, and J. Brugger, Adv. Mater. 32(31), 2001232 (2020).
- 107 X. Zheng, A. Calò, E. Albisetti, X. Liu, A. S. M. Alharbi, G. Arefe, X. Liu, M. Spieser, W. J. Yoo, T. Taniguchi, K. Watanabe, C. Aruta, A. Ciarrocchi, A. Kis, B. S. Lee, M. Lipson, J. Hone, D. Shahrjerdi, and E. Riedo, Nat. Electron. 2(1), 17 (2019).
- <sup>108</sup>M. Wang, D. Li, K. Liu, Q. Guo, S. Wang, and X. Li, ACS Nano 14(9), 11169 (2020).